EUROPEAN ORGANIZATION FOR NUCLEAR RESEARCH

CERN PPE/92-187
6 November, 1992

The Small Angle Spectrometer of Experiment UA8 at the SppS-Collider

A. Brandt[1], J. Ellett, S. Erhan, R. Jackson, A. Kuzucu[2], M. Medinnis,
P. Oillataguerre†, N. Ozdes[2], P. Schlein, M. Zeyrek[3], J. Zweizig
University of California*), Los Angeles, U.S.A.

J.B. Cheze, J. Zsembery
Centre d'Etudes Nucleaires-Saclay, 91190 Gif-sur-Yvette, France

Abstract

Experiment UA8 at the SppS-Collider studied the production of hadronic jets in $p\bar{p}$ interactions which also contained final state protons or anti-protons with more than 90% of the full beam momentum of 315 GeV. Four Roman pot spectrometers were installed in interaction region LSS4 and interfaced to the data acquisition system of the UA2 calorimeter experiment, such that UA8 data could be logged on UA2 raw data tapes. In order to minimally perturb normal UA2 data acquisition and allow concurrent operation for the life of the experiment, an efficient high speed data-driven trigger processor was employed. The processor calculated the momentum of a track in a Roman pot spectrometer with 1.4% accuracy in 450 nsec, thereby allowing a trigger decision to be made within 1.3 μsec. We describe the integration of this processor into the high bandwidth readout of the UA8 wire chamber TDC system, and the online software package which monitored the hardware operation. The suppression of backgrounds from beam halo and multiple interactions in a bunch crossing is also discussed.

Submitted to Nuclear Instruments and Methods

---

*) Supported by U.S. National Science Foundation, Grants PHY90-08221 and PHY85-09175.
† Deceased.
1) Now at Fermi National Accelerator Laboratory, Batavia, IL.
2) Visitor from Cukurova University, Adana, Turkey; also supported by ICSC - World Lab.
3) Visitor from Middle East Technical University, Ankara, Turkey.

Contents

1 Introduction

The main goal of the UA8 Experiment was the study of the hadronic jet structure of events produced in proton-antiproton collisions which also contained a forward proton or antiproton in the final state, which possessed more than 90% of the full beam momentum of 315 GeV. These final state "leading" particles were measured in four Roman pot spectrometers located in the LSS4 intersection region of the CERN Sp$\bar{p}$S-Collider. The energy flow structure was measured in the upgraded calorimeter system of the UA2 experiment[1]. The UA8 spectrometers were interfaced to the UA2 data acquisition system such that the UA8 data could be logged on UA2 raw data tapes together with the UA2 detector data from the same event.

The trigger required a coincidence between a recoil proton or antiproton signature in one of the spectrometers and a minimum total transverse energy in the UA2 calorimeter system. The use of scintillators alone to signal the presence of a recoil proton in the spectrometers led to a trigger rate which was several orders-of-magnitude larger than the rate expected from the known cross sections for these processes. Undesirable triggers resulted from low momentum particles, beam halo particles traversing the spectrometers, or accidental coincidences of hits from different tracks.

To eliminate these sources of spurious triggers and lower the trigger rate to a level acceptable for concurrent operation with UA2, a 240 MIPS data-driven trigger processor[2] (four 60-MIPS processors running in parallel) was designed to reconstruct and calculate the momentum and initial direction of trigger particles using its measured wire chamber coordinates and the system geometry constants. These reconstructed quantities were required to lie within predetermined limits and a decision was produced in 450 nsec. When the time to read out the wire chamber system is included, a trigger was available to UA2 in less than 1.3 μsec after a Bunch-Crossing RF signal arrived in the counting room.

The UA8 spectrometers are described in Chapter 2. The trigger and readout system is in Chapter 3. The associated online software packages used for setting up the triggers for data acquisition and for monitoring the TDC-Processor hardware operation are in Chapter 4. The procedures used to suppress backgrounds from halo tracks and from pileup (multiple interactions in a bunch crossing) are discussed in Chapter 5. Finally the system performance is described in Chapter 6.

Table 1 contains a list of the various physics triggers used in the experiment. The first observations[3] of jet production in events with leading protons ("Proton-ΣE_t" trigger) resulted from an early test run of this experiment in 1985 using prototype wire chambers and no trigger processor. The final UA8 results on this subject have been submitted to Physics Letters[4]. Results from Single Diffractive Excitation ("Proton" trigger) and on Double Pomeron Exchange, in which the UA2 calorimeter system is used to study the energy flow in the diffractively excited systems, are found in Refs. [5, 6].

During the course of the UA8 experiment, we discovered that the Roman pot spectrometers

could also be used to measure Λ° or $\overline{\Lambda^\circ}$ particles which possessed more than about 70% of the beam momentum. The construction and use of a trigger which was implemented to study $\overline{\Lambda^\circ}$ production will be reported elsewhere[7], together with the measurements it produced.

This description of the methods used in the development and integration of our triggers with the standard UA2 high-p_t triggers may be of use in future efforts of this type at other $p\bar{p}$, ep or pp colliders.

2 The Spectrometers

2.1 Layout

The UA8 apparatus consisted of four independent, identical spectrometers positioned above and below both outgoing arms of the Sp$\bar{p}$S beam pipe in LSS4. One of the outgoing arms (two spectrometers) is sketched in Fig. 1 and contains four Roman pot assemblies[8] located between 13 m and 33 m from the interaction region. Bending for momentum analysis was provided by the pairs of machine quadrupole magnets Q_1 and Q_2 in Fig. 1 and, to a lesser extent, by the pair Q_3 and Q_4. The major difference between the UA8 pot configuration shown in Fig. 1 and that used earlier by experiment UA4[8] is that our first pot is installed in front of Q_1 to allow acceptance of particles with momentum 285 GeV and below and to facilitate online track reconstruction without the need to assume a vertex position. The first three pots yield an adequate momentum resolution (see below) and traversal through the fourth pot is not required.

Fig. 2 shows particle trajectories through a Roman pot spectrometer. The solid curves are trajectories of 300 GeV particles emerging from the center of the intersection region with minimum and maximum acceptable angles. The lower edge of the shaded region on this figure is 12 beam widths (σ) from the beam center, while the upper edge shows the trajectory of the largest angle elastic track (315 GeV) which remains inside the vacuum pipe. Lower momentum tracks which pass below pot 4 could also be reconstructed and analyzed. Vertical lines show the positions of the pots 1 through 4 from the intersection region. Q_1 and Q_2 focus vertically. Since particles are further from the beam axis in this set than in Q_3 and Q_4, they traverse a region of higher magnetic field and thus are deflected through larger angles. For this reason, the first three Roman pots coupled with Q_1 and Q_2 yield a substantially better momentum measurement than do pots 2, 3 and 4 with Q_3 and Q_4. The momentum resolution is further discussed in Sect. 6.2.

The Roman pots used for UA8 are cylindrical stainless-steel pots or containers, 26 cm in diameter and 24.5 cm in depth, which allow detectors to function close to the beam, but outside the machine vacuum. Particles traverse 100 μm stainless steel windows at the entrance and exit of each pot. A vertical slice through a Roman pot with its mounted detectors is shown in Fig. 3. Each Roman pot contained a 6-plane mini-drift proportional wire chamber, described in the following section, and a 5 cm square plastic scintillator which was used for triggering and event timing. Fig. 4 shows a photograph of a complete detector assembly.

The pots could be displaced in the vertical direction under remote control. During periods of unstable beam conditions the pots were retracted, leaving approximately 8 cm between the nominal beam position and the bottom of the pot. During data taking, the bottom of each pot was positioned a fixed number of beam widths (σ) from the nominal beam line, where σ was calculated assuming the average beam emittance of $\epsilon = 2 \times 10^{-5}\,\pi$ meter·rad. For most of the running, the pots were positioned at a conservative $14\,\sigma$, although we sometimes ran with the pots as close as $12\,\sigma$ with negligible effect on UA2 background rates and no discernable effect on other experiments.

For alignment purposes, all vertical distances are referred to a circular horizontal flange at the top edge of each pot. The flat surface of this flange is aligned to the horizontal plane with an accuracy of 0.1 mrad. The vertical position of the flange is monitored with a linear potentiometer with accuracy in absolute position of 100 μm. Pot displacements cause the flange to wobble about the vertical axis by less than 0.1 mrad. The potentiometer is calibrated by a micrometer which is permanently fixed to the side of the pot-positioning mechanism. The pots could be retracted and repositioned with a precision better than 50 μm.

Contour plots of the acceptance for one of the spectrometers as a function of Feynman-x, x_p, of the detected proton or antiproton and four-momentum transfer, t, are shown in Fig. 5. The domain of good acceptance extended from 0.8 to 2.5 GeV^2 in t and from 0.7 to 1.0 in x_p.

2.2 Mini-Drift Wire Chambers

The chamber aperture was determined by the requirement that it not limit the spectrometer acceptance. As seen in Fig. 2, the maximum excursion of particles from the beam line occurred in the first set of quadrupole magnets. A vertical chamber aperture of 53 mm ensured that the acceptance was limited by the beam-pipe aperture for any possible Roman-Pot position. A horizontal aperture of 60 mm was chosen based on similar considerations.

The anode and cathode configurations are typical of conventional multi-wire-proportional chambers (MWPC) with 2 mm anode wire spacing. Short drift times were required, since chamber hit information was used in the trigger. The signals were interfaced to a "mini-drift" Time-Digital-Converter (TDC) system, with one TDC channel for each wire. This system, described in Sect. 3.3, was used with an 80 nsec gate and had 4-bit timing information with a 5 nsec least count.

Although such chambers have a non-uniform electric field distribution in the drift region, a substantial gain in point resolution can be realized by measuring the arrival times of hit signals. Fig. 6 shows an empirical point-of-impact vs. drift time dependence for these chambers. This dependence was inferred from the observed distribution of drift times, with the assumptions that the track distribution is uniform across a cell, and that the jitter produced by ionization statistics is small. The time, t_0, at which a track traverses a chamber plane, is estimated using the scintillator-hit times. The average point-of-impact, $x(t)$, as a function of the corrected drift

time is estimated, using a large track sample, as the fraction of all hits with corrected drift time less than t, multiplied by the half-width of a drift cell (0.1 cm). The turnover at low drift times in Fig. 6 is a consequence of the finite resolution of the t_0 estimate.

Each chamber consisted of 6 anode wire planes separated by graphite-coated mylar cathodes. The six planes were organized into three views of 2 planes each (y, $\tilde{y}$, u, $\tilde{u}$, v, $\tilde{v}$). The wires of the $\tilde{y}$, $\tilde{u}$ and $\tilde{v}$ planes were displaced by a half-wire spacing of 1 mm from the y, u and v planes to solve the intrinsic left/right ambiguities. The anode wires of y-view planes were horizontal while the u (v) planes were oriented at +7 (-7) degrees from the horizontal. This rather shallow stereo angle was chosen since it improved resolution in the vertical (bending) view while maintaining adequate resolution in the horizontal view[1].

The support frames for anode and cathode planes consisted of single pieces of 116 x 95 mm, 1/8 inch thick G-10 (Vetronite), from which rectangular windows of 64 x 62 mm were machined. The anode planes were copper-clad on one side. Only 0.5 mm of frame material was retained on the side closest to the beam, in order to achieve acceptance at the smallest possible scattering angle. Additional holes were machined for alignment pins, bolts and gas circulation. Solder pads for the anode wires and traces leading to a vertical edge, configured to accept a standard card-edge connector, were etched from the copper-clad surface of the anode cards before machining.

The 2 mm anode-wire spacing was assured by forcing each wire to pass through grooves machined to a precision of $\pm 10\,\mu$m into epoxy-resin strips which were glued near the two vertical sides of the window frame. The location of these strips relative to the alignment pins was measured under a microscope.

The anode and cathode planes along with aluminized-mylar outer windows were sandwiched between two 25 mm thick aluminum mounting plates from which matching windows had been machined. To ensure a gas tight volume, the two sides and top of the assembly were enclosed with copper-clad G-10 and the side closest to the beam by a thin copper plate. Joints were sealed with adhesive copper tape. Three card edge connectors mounted on each side piece carried the anode signals from the six wire planes to the outside of the box.

The spatial resolution of the mini-drift chambers is found to be about 160 μm per plane. Six planes together provide a point resolution in the vertical bending plane of about 65 μm. In the horizontal plane, the point resolution is about 670 μm. The large difference between these numbers is a consequence of small stereo angle used.

Efficiencies were measured for each wire in the chamber system. In general, the wire efficiencies are greater than 98%, except near the chamber edges. Typically, the efficiency rises from zero at the chamber edge to over 98% about 2.5 mm from the chamber edge.

[1]The horizontal x-view measurement was needed primarily to determine the scattering angle and momentum transfer. Since the beam was tuned for high luminosity, beam dispersion dominated the scattering angle error.

from the TDC half-crates (via the Readout modules) to the Memory modules is controlled by the Control (CTRL) module which occupies one of three special slots in the backplane of the Memory crate. The data in the Memory modules were also accessible to the UA8 μVAX for diagnostic and control functions (see Chapter 4), via the diagnostic bus shown in Fig. 8.

Hits were transferred to the Memory modules at the rate of 1 hit/90 ns. With simultaneous readout of the sixteen UA8 chambers, a peak bandwidth of 360 MBytes/sec was achieved (in the full system[11] used in ISR Experiment R608, the bandwidth was larger than 1 Gbyte/sec).

The Memory modules were interfaced to the UA2 data-acquisition system via a TDC Buffer Readout Controller (TBRC) module[12], which resided in one of the special Memory crate slots, as shown in Fig. 8. The TBRC is a synchronous state machine which polls the Memory modules and sends all recorded hits over a Remus VBUS at the maximum RWBD I/O rate.

3.4 Data-Driven Trigger Processor

The momentum calculation is described in the following section. Following that are descriptions of the two types of modules which implemented the calculation. Detailed technical descriptions of the modules are given in References [2, 12].

3.4.1 Momentum Calculation

The starting point for the momentum calculation is the following equation[3], which relates the vertical position (y_f) of a track at position f, to the vertical position (y_i) and slope (y_i') at position i, in the presence of a set of quadrupole magnets and field-free drift spaces between positions i and f:

$$y_f = R_{33}y_i + R_{34}y_i' + \Delta \cdot (T_{336}y_i + T_{346}y_i') \tag{1}$$

where Δ is the fractional momentum difference from the central beam momentum p_0 and the coefficients R_{33}, R_{34}, T_{336} and T_{346} are calculated from the magnet parameters for a particle of momentum p_0.

As shown in Ref.[2], with the relation $\Delta = ln(e^{\Delta}) \approx ln(1 + \Delta)$ for small Δ, Eq. 1 can be solved for Δ in terms of the track's vertical coordinates in the first 3 chambers, y_1, y_2 and y_3, and four known constants, a, b, c and d:

$$\begin{aligned} \Delta &= \ln(C) - \ln(B) \\ C &= y_1 + A \\ A &= a \cdot y_2 + b \cdot y_3 \\ B &= c \cdot y_2 + d \cdot y_3 \end{aligned} \tag{2}$$

[3]The notation used here is that used by the TRANSPORT beam optics program[13].

time is estimated, using a large track sample, as the fraction of all hits with corrected drift time less than t, multiplied by the half-width of a drift cell (0.1 cm). The turnover at low drift times in Fig. 6 is a consequence of the finite resolution of the t_0 estimate.

Each chamber consisted of 6 anode wire planes separated by graphite-coated mylar cathodes. The six planes were organized into three views of 2 planes each (y, $\tilde{y}$, u, $\tilde{u}$, v, $\tilde{v}$). The wires of the $\tilde{y}$, $\tilde{u}$ and $\tilde{v}$ planes were displaced by a half-wire spacing of 1 mm from the y, u and v planes to solve the intrinsic left/right ambiguities. The anode wires of y-view planes were horizontal while the u (v) planes were oriented at +7 (-7) degrees from the horizontal. This rather shallow stereo angle was chosen since it improved resolution in the vertical (bending) view while maintaining adequate resolution in the horizontal view[1].

The support frames for anode and cathode planes consisted of single pieces of 116 x 95 mm, 1/8 inch thick G-10 (Vetronite), from which rectangular windows of 64 x 62 mm were machined. The anode planes were copper-clad on one side. Only 0.5 mm of frame material was retained on the side closest to the beam, in order to achieve acceptance at the smallest possible scattering angle. Additional holes were machined for alignment pins, bolts and gas circulation. Solder pads for the anode wires and traces leading to a vertical edge, configured to accept a standard card-edge connector, were etched from the copper-clad surface of the anode cards before machining.

The 2 mm anode-wire spacing was assured by forcing each wire to pass through grooves machined to a precision of $\pm 10\,\mu$m into epoxy-resin strips which were glued near the two vertical sides of the window frame. The location of these strips relative to the alignment pins was measured under a microscope.

The anode and cathode planes along with aluminized-mylar outer windows were sandwiched between two 25 mm thick aluminum mounting plates from which matching windows had been machined. To ensure a gas tight volume, the two sides and top of the assembly were enclosed with copper-clad G-10 and the side closest to the beam by a thin copper plate. Joints were sealed with adhesive copper tape. Three card edge connectors mounted on each side piece carried the anode signals from the six wire planes to the outside of the box.

The spatial resolution of the mini-drift chambers is found to be about $160\,\mu$m per plane. Six planes together provide a point resolution in the vertical bending plane of about $65\,\mu$m. In the horizontal plane, the point resolution is about $670\,\mu$m. The large difference between these numbers is a consequence of small stereo angle used.

Efficiencies were measured for each wire in the chamber system. In general, the wire efficiencies are greater than 98%, except near the chamber edges. Typically, the efficiency rises from zero at the chamber edge to over 98% about 2.5 mm from the chamber edge.

[1]The horizontal x-view measurement was needed primarily to determine the scattering angle and momentum transfer. Since the beam was tuned for high luminosity, beam dispersion dominated the scattering angle error.

2.2.1 Chamber Electronics

The amplifier card for each wire plane contained 32 channels, each with four cascaded capacitively-coupled amplification stages utilizing Motorola MC10115 ECL line receivers, followed by MC10116 line-drivers. The 10116s also served as comparators, in that their inputs were biassed by +200 mV, such that an amplified signal of −300 mV produced a full differential logic swing at the output. The overall gain of the four cascaded amplification stages could be adjusted from a maximum of 1500 down to 800 or less by decreasing the value of V_{EE} from its nominal value of -5.2 Volts down to about -4.8 V. We typically ran with about -4.9 V, with the advantage that heat generation was reduced. Anode signals above a 0.3 mV threshold produced differential ECL logic pulses. These signals were sent to the counting room over 70 m long flat polyethylene cables manufactured by Ansley. Every third wire of the 101-conductor cables was grounded to prevent cross-talk.

3 Triggers and Readout

3.1 Architecture

The UA8 trigger combined scintillator, processed chamber hit information, the ΣE_t signal from the UA2 calorimeter, and the Bunch-Crossing RF signal (from a directional coupler mounted near the intersection) to produce 9 independent trigger decisions, which were prescaled and OR'ed together to form the global UA8 trigger. When data acquisition was performed by UA2, this trigger was in turn OR'ed with the UA2 high p_t triggers. A block diagram of the UA8 trigger and readout system is shown in Fig. 7.

The triggering sequence was initiated by the arrival of the RF signal which generated several strobes timed to coincide with the arrival of chamber hits and scintillator hits from particles emerging from interactions. Other appropriately timed strobes were used to latch scintillator hits from beam halo particles. These signals were used in veto to remove the halo background discussed in Chapter 5.

The digitized wire chamber hit data were transferred to hit buffers starting 80 nsec after the arrival of the RF signal and simultaneously latched into the trigger processor. Approximately 1 μsec after arrival of the RF signal, the processor outputs were combined with the latched scintillator hit information and ΣE_t signals from UA2 in the NIM Trigger Logic to produce the UA8 triggers.

As discussed below in Chapter 4, the UA8 online computer was used during standard data-taking to configure the trigger processor, to enable or disable triggers, to change trigger conditions and to monitor data which were being written on tape.

Readout was based on the CERN Romulus/Remus[9] system, which is capable of autonomous data collection. Each crate of CAMAC data encoders is controlled by a Read/Write Crate

Controller (RWCC). The RWCC scans through all modules in the crate according to one of 16 standard procedures. Up to 16 such crates may be daisy-chained together in a branch. Each such branch or Vertical Bus (VBUS) is in turn read out by a Read/Write Branch Driver (RWBD) CAMAC module. As discussed in Sect. 3.3, an RWBD module also read out our wire chamber TDC system via a so-called TBRC module.

3.2 Interface to Experiment UA2

The UA8 and UA2 fast electronics were synchronized using a trigger signal, sent by UA8 to UA2 when an event satisfied the trigger requirements summarized in Sect. 3.5, and a reset signal which was sent from UA2 to UA8. When no reset signal appeared before the RF signal, as was the case when an event had been triggered by UA2, the UA8 fast electronics blocked further readout cycles and trigger calculations until UA2 was ready.

The UA8 online μVAX computer shared the Remus tree structure with the UA2 computer by means of a Romulus Router Unit[10]. Thus, the UA8 computer could be either the readout master, for testing and stand-alone data acquisition, or a Spy when monitoring the UA8 detector data being read by UA2. A Romulus buffer module was installed between the Router and RWBD modules to decouple the two channels when in Spy mode. A data-available status flag generated by the buffer module was used to initiate data acquisition by the UA8 μVAX.

3.3 The Chamber TDC and Hit-Buffer System

The TDC and Hit-Buffer system shown in Fig. 7 and, in more detail, in Fig. 8, was originally designed and manufactured at UCLA for ISR experiment R608[11]. The entire system is implemented using ECL logic. Drift times are digitized and the addresses of those wires whose signals arrive during an 80 nsec gate are encoded. The system reads out only the addresses and drift times of hit wires ("sparse-data-scanning"). Sixteen high-speed parallel data paths connect the TDC modules to eight hit-buffer or Memory modules via the Readout modules (MEM & RO, respectively, in Fig. 8).

One 32-channel TDC module receives the signals from each wire plane. In the UA8 configuration, all 6 TDC modules for a given chamber were placed in a single half-crate, ordered such that the y and $\tilde{y}$ planes were read out first. The time digitization is accomplished by latching the state of a 4-bit Gray-code counter upon arrival of a hit[2]. The Gray-code clock signals, with 5 nsec time bins, are generated in each half-crate by the Readout module in Fig. 8. Only one hit per wire can be latched for each event.

As seen in Fig. 8, the Memory modules for all TDC modules are located in a single "Memory" crate. Two hit-buffers, each capable of storing up to thirty-one 16-bit hit words from a half-crate of TDC modules, are contained on a single Memory module. The parallel transfer of hit data

[2]This technique was developed by W. Sippach, Nevis Laboratories, Columbia University.

from the TDC half-crates (via the Readout modules) to the Memory modules is controlled by the Control (CTRL) module which occupies one of three special slots in the backplane of the Memory crate. The data in the Memory modules were also accessible to the UA8 μVAX for diagnostic and control functions (see Chapter 4), via the diagnostic bus shown in Fig. 8.

Hits were transferred to the Memory modules at the rate of 1 hit/90 ns. With simultaneous readout of the sixteen UA8 chambers, a peak bandwidth of 360 MBytes/sec was achieved (in the full system[11] used in ISR Experiment R608, the bandwidth was larger than 1 Gbyte/sec).

The Memory modules were interfaced to the UA2 data-acquisition system via a TDC Buffer Readout Controller (TBRC) module[12], which resided in one of the special Memory crate slots, as shown in Fig. 8. The TBRC is a synchronous state machine which polls the Memory modules and sends all recorded hits over a Remus VBUS at the maximum RWBD I/O rate.

3.4 Data-Driven Trigger Processor

The momentum calculation is described in the following section. Following that are descriptions of the two types of modules which implemented the calculation. Detailed technical descriptions of the modules are given in References [2, 12].

3.4.1 Momentum Calculation

The starting point for the momentum calculation is the following equation[3], which relates the vertical position (y_f) of a track at position f, to the vertical position (y_i) and slope (y_i') at position i, in the presence of a set of quadrupole magnets and field-free drift spaces between positions i and f:

$$y_f = R_{33}y_i + R_{34}y_i' + \Delta \cdot (T_{336}y_i + T_{346}y_i') \tag{1}$$

where Δ is the fractional momentum difference from the central beam momentum p_0 and the coefficients R_{33}, R_{34}, T_{336} and T_{346} are calculated from the magnet parameters for a particle of momentum p_0.

As shown in Ref.[2], with the relation $\Delta = ln(e^{\Delta}) \approx ln(1 + \Delta)$ for small Δ, Eq. 1 can be solved for Δ in terms of the track's vertical coordinates in the first 3 chambers, y_1, y_2 and y_3, and four known constants, a, b, c and d:

$$\begin{aligned} \Delta &= \ln(C) - \ln(B) \\ C &= y_1 + A \\ A &= a \cdot y_2 + b \cdot y_3 \\ B &= c \cdot y_2 + d \cdot y_3 \end{aligned} \tag{2}$$

[3]The notation used here is that used by the TRANSPORT beam optics program[13].

The calculation is thus reduced to a set of four calculations, each of which is the sum of two single variable functions. As discussed below in Sect. 6.2, an online momentum error of 4.0 GeV or 1.4% was obtained in this calculation.

3.4.2 Intercept and Momentum Transfer Calculations

Two additional calculations were also performed by the processor. One was the y-intercept of a track at the center of the interaction region ($z = 0$). However, the y-intercept distribution was rather clean and the calculation lead to no substantial additional background suppression. It was therefore not used during data taking.

The 4-momentum transfer to a proton which has a small scattering angle is given by t $\sim$ $pp_0\theta^2$, where p is the track's momentum and p_0 is the central beam momentum. The calculation was implemented in the processor by imposing limits on both p and the track slope ($y' \approx \theta$). The effectivenesss of this trigger condition is illustrated in Fig. 11 and discussed in Sect. 3.4.5.

3.4.3 Dual-Input Memory-Lookup and Summation Module (DIMSUM)

Each line of Eqs. 2 can be executed in a module that has 2 independent digital inputs, a table look-up for each, and a summation of the two table outputs. A general-purpose module, called DIMSUM (for Dual Input Memory-Lookup and Summation) was designed for this purpose. By interconnecting DIMSUM modules into a multi-layered network, arbitrarily complex calculations can be performed.

Since the calculations of A and B in Eqs. 2 may be performed simultaneously, the entire momentum calculation can be made in 3 module delays, as shown in Fig. 9. The evaluation of a track's slope for the momentum transfer calculation requires only 2 additional DIMSUM modules which function in parallel with the momentum calculation, therefore taking no additional time.

As described in the next section, the EDSEL module and the first layer of DIMSUM modules shown in Fig. 9 produce the three y coordinates which are used in the momentum calculation. The quantity , Δ, is output from the calculation, together with the result of the slope calculation (not shown in Fig. 9). They are input to one final DIMSUM module which makes the final event selection as discussed below in Sect. 3.4.5.

The DIMSUM module is implemented with TTL logic and housed in a single width CAMAC module. All numeric data propagate asynchronously between modules along 26-wire flat cables which connect to the DIMSUM's front panels. A DIMSUM output stabilizes approximately 100 nsec after signals appear at the module inputs. The total transit time through the processor shown in Fig. 9 is about 450 nsec. Counting the effective number of instructions in each DIMSUM module leads to an effective computing power of about 60 MIPS per processor. With the four UA8 processors operating in parallel, the total capability is 240 MIPS. Each of the processors were housed in one CAMAC crate.

The functional blocks of the DIMSUM module are shown in Fig. 10. The DIMSUM module has two operational modes, online and offline, respectively, controlled by the host computer through the CAMAC interface. In the online mode, each 12-bit input word addresses a 4096 x 14 bit RAM. The sum of the first 12 bits of the two addressed words is output on a 12-bit bus. Offline, in a test and load mode, RAM data can be entered or read via the CAMAC interface.

Each module contained parity and overflow checking circuitry which could be daisy-chained to obtain a single system-wide error signal. The system reliability proved to be so high, as judged from the online monitoring utilities, that this error signal was never used.

Software utilities for emulating the DIMSUM system as well as loading, monitoring, testing, and facilitating the repair of the system are described in Chapter 4.

3.4.4 Event Data Selector (EDSEL)

A second type of module, called EDSEL (Event Data SELector), interfaced the chamber TDC system to the first layer of DIMSUM modules. As shown in Fig. 8, the EDSEL inputs tapped on to the cables which transfer chamber hits from the TDC system to the Memory modules. One EDSEL module was used for each of the first 3 chambers in each spectrometer.

Each EDSEL module generated a Data Valid signal for events in which the hit configuration in the y and $\tilde{y}$ planes was consistent with a single track traversal (one or two contiguous hits in both planes, with y and $\tilde{y}$ addresses differing by at most one wire). The Data Valid signals for all modules were sent to the NIM Trigger Logic for use in the final trigger decision.

From each EDSEL module, the latched y-plane hit addresses, y and $\tilde{y}$ time codes and ambiguity variable (which indicates the drift direction, based on whether the hit coordinate in the $\tilde{y}$ plane is larger or smaller than that in the y plane) were sent on two cables to a DIMSUM module for calculation of the y-coordinate. One cable carried the address of the hit y-plane wire which was converted to a y position by table look-up. The other cable contained the time codes and ambiguity variable, from which a signed drift distance was computed. The DIMSUM module outputs the sum of these two quantities, which is the y coordinate.

The EDSEL module is housed in a single width CAMAC module. It was periodically tested by sending simulated hit data through the CAMAC dataway. During the course of the experiment, data was periodically recorded for calibration purposes with no EDSEL or DIMSUM requirements in the trigger.

3.4.5 Limit Comparisons and Trigger Suppressions

The DIMSUM processor system is capable of simultaneously producing several trigger decisions based on different sets of requirements imposed on the results of the calculation. For example, in the final DIMSUM module in Fig. 9, this was accomplished by assigning a pair of adjacent bits in the DIMSUM output word to each trigger. Both lookup tables were set up such that the low-order bit of each trigger bit pair was set "on" for all input values within the valid

range for that trigger. After addition of the two table lookup outputs, the high-order bit of each pair is the logical AND of the two trigger tests. These bits are then transmitted to to the NIM Trigger Logic, which is discussed in the following section.

Table 1 lists the various triggers used in the experiment, along with their requirements and raw trigger rates. The rate suppressions shown in the table illustrate the overall capability of the processor system. Not shown in the table is the fact that the "Proton" trigger rate was reduced by a factor of $\sim$ 150 from the raw scintillator concidence rate by demanding that events pass the basic EDSEL and DIMSUM requirements, before including a cut on the track momentum.

Fig. 11 shows the offline calculated momentum transfer for Proton-ΣE_t triggered events and for those that also satisfy the High-t trigger requirement. The rate suppression between the Proton-ΣE_t and High-t triggers shown in Table 1 is about a factor of 30, although Fig. 11 shows that the t-range selected by this trigger reduces the sample by about a factor of 10. The additional factor of 3 arises because of the more restrictive momentum selection made for the High-t trigger.

3.5 NIM Trigger Logic

The NIM Trigger Logic system was responsible for overall synchronization of the trigger with the Beam-Crossing signal and data-acquisition system as well as the generation of a global trigger decision which initiated either a reset signal or an interrupt to the UA2 or UA8 data-acquisition systems.

All UA8 triggers could be recorded simultaneously, each with a pre-scale factor for independent trigger rate adjustment. Under normal running conditions, a "Track" in Table 1 was required to satisfy the following conditions:

- EDSEL Data Valid,
- DIMSUM momentum and slope in specified range,
- scintillator signals in pots 1, 2, 3,
- no scintillator signals in pots 1 and 2 of the other spectrometer in the trigger arm ("Opposite Veto"),
- no scintillator "halo" signals in pots 1 and 2 of diagonally opposite spectrometer ("Halo Veto").

Almost the entire logic circuit was implemented with several examples of a UCLA-designed NIM module called "LOGICBOX". The LOGICBOX used PAL circuitry which allowed condensing several layers of traditional NIM logic units into a single unit while simultaneously increasing flexibility by explicitly providing for computer control of the trigger circuit. The entire UA8

trigger logic fit into three NIM crates which also housed discriminators for scintillator signals, visual scaler drivers and several units devoted to generating strobes and timing signals.

The double width LOGICBOX module has a front panel with Lemo 00 connectors for 24 NIM inputs and 24 NIM outputs as well as eight TTL inputs (on two 4-pin Lemo connectors) which are used for computer control of trigger conditions. The 24 NIM inputs are separated into three groups of eight signals. The inputs are converted to TTL levels and latched using a common (externally generated) strobe for each octet.

The outputs of the latches are available on wire-wrap pins located on the periphery of a "bread-board" section, on which is built a PAL (Programmable Array Logic) logic circuit[4], typically with two or three PALs per module. 24 wire-wrap pins are available for connecting outputs from the PAL logic section to a bank of TTL to NIM converters whose outputs appear on front panel Lemo 00 connectors. The input to output delay of the LOGICBOX is dominated by the approximately 25 nsec propagation time through each level of PALs.

4 Online Software

The UA8 online software consists of 3 packages which perform the following functions: (i) Data-Acquisition and Monitoring, (ii) Trigger Setup and (iii) Readout and Trigger Diagnostics. This software was run on a μVAX II computer with 2 Megabytes of memory, a CAMAC interface and two Storage Technology 6250 BPI tape drives.

4.1 The Data Acquisition and Monitoring Programs

The UA8 online system was used primarily for monitoring data which was read and logged by the UA2 data acquisition system and, periodically, for recording calibration data. It is structured as a set of independent processes which communicate via the VAX/VMS mailbox mechanism for control and status information, and via a Global Common Area for event data transfer. Each process performs a specific data-acquisition or monitoring function. Task scheduling is performed by the VAX/VMS process scheduler.

Event data are read into one of several global event buffers by the Data Acquisition Task. This task reads the data when activated by an event interrupt asserted through the CAMAC controller. After readout, an event buffer in the Global Common Area is allocated to all processes (consumers) which have pending event requests. The buffer contents are kept intact until all consumers have copied the event to local buffers.

Data acquisition and monitoring are controlled by the physicist through the Command and Status Program (CSP). CSP commands allow the starting and stopping of monitoring, data acquisition and recording processes, setting of acquisition parameters, and viewing of status summaries and histograms produced by the active consumers. Several users may run CSP

[4]For most purposes, the erasable 22V10 PAL, manufactured by Cypress was used.

concurrently to monitor the same or different parts of the experiment, without interfering with one another. A macro facility allows commonly used sequences of commands to be executed by a single command.

Error messages are sent from active processes to the error logging task, LOGGER, which keeps a copy of all messages produced during a run, and forwards the message text to all enabled CSP processes. One of the event consumers is a recording process, TAPE, which writes all events with the selected trigger type(s) to either a disk or tape file.

Offline debugging of data-acquisition and monitoring code was facilitated by a Monte Carlo event source. All routines that communicate directly with the detectors or the trigger electronics are replaced by an interface to the UA8 Proton trigger Monte Carlo event generator. Generated events could thus be passed to the acquisition and monitor routines via the same data paths used for real events.

The monitor processes are based on the UA8 offline analysis program with the event input routine replaced by one which reads data directly from the event buffer. The only difference between an online monitor and an offline analysis routine is in the definition of parameters which may be set interactively using CSP and the addition of an optional display formatting routine.

Imbedding the online monitor routines within the offline program results in a more integrated and more easily learned structure while insuring that all software written can be used in both online and offline environments. The monitor routines include those that verify the event structure, monitor the trigger performance, accumulate and display trigger and other rates from the scaler blocks, and perform complete track reconstruction and histogramming.

4.2 Trigger Setup

The trigger was initialized at the start of each $Sp\bar{p}S$ fill by running a menu driven setup routine, TRGSET. The Roman pot positions were read from the $Sp\bar{p}S$ control computer and the DIMSUM table contents were calculated.

Upon exit, TRGSET loaded the DIMSUM tables, set the LOGICBOX control registers and the programmable ΣE_t discriminators with the desired trigger settings. With the exception of the Roman pot positions, the trigger parameters were changed infrequently. Thus the setup procedure normally involved only a routine check followed by the calculation and loading of the settings, a process which took about two minutes.

4.3 Readout and Trigger Diagnostics

Test and maintenance routines were developed for the chamber readout system, TBRC-Remus interface and trigger-processor system. Their purpose was to test, as completely as possible, every latch and data path in the system. The various systems were also monitored by CSP consumers during data acquisition.

A test routine for the chamber TDC readout system, which was usually run just before, and immediately after each Sp$\bar{p}$S coast, tested all cards in the readout tree structure. Another program, which was useful for isolating and diagnosing faults, allowed the user to interactively perform most of the primitive operations, such as zeroing hit latches, setting TDC clocks, latching times on even- or odd-numbered TDCs or reading hits to memory. A third program addressed the most common failure mode for the system: the failure of a memory chip on a Memory module. This routine wrote a series of patterns to all the memories and read them back. If an error was found, the faulty chip was identified, and its position on the board was indicated.

All trigger-processor system diagnostics were contained in a single program which could be run interactively or in batch mode. The package included specific test routines for each module type (EDSEL and DIMSUM), plus a system integrity test which verified module interconnections. If an error was found, an error page was printed which contained the error code, the module name and address, and a trace table indicating the last eight operations in the current step of the test procedure and their results. The procedures optionally repeated the failing step continuously to facilitate the diagnosis of the fault. The entire test required about 45 minutes, and was run twice a week.

5 Pileup and Halo Background Rejection

In this section we describe how the available detectors could be used offline to suppress background from pileup and from halo tracks.

Pileup Rejection A major source of background for the Proton-ΣE_t triggers comes from two superimposed events ("pileup"), with one event contributing a diffractively scattered proton or antiproton and the other contributing enough energy to the UA2 calorimeter to satisfy the ΣE_t requirement. The same background also contributes to the other triggers, although to a lesser extent.

We found four ways to effectively suppress this background:

1. The arrival times measured by the UA2 time-of-flight (TOF) counters[1], which covered the pseudorapidity range 2.3-4.1 in both arms, were required to be consistent with a single event hypothesis. This check was implemented primarily by finding the event time, t_0, and its vertex position, z, which minimized the following χ^2:

$$\chi^2 = \sum_{i=1}^{N} \frac{[t_0 + |Z_i - z|/c - t_i]^2}{\sigma_i^2} \tag{3}$$

where N is the number of hit TOF counters, t_i is the time of the i'th hit counter, Z_i is its coordinate and σ_i is its time resolution.

2. The UA2 time-of-flight counters and UA8 scintillation counters were required to give consistent event times. The t_0 and z found in the previous paragraph are used to test if the quantity,

$$\delta t = t_0 + |Z_{UA8} - z|/c - t_{UA8} \quad (4)$$

is less than 1 nsec. Z_{UA8} is the coordinate of the UA8 scintillation counters.

3. Events were required to have no more than one event vertex, as determined by the UA2 silicon detector analysis.

4. A cut was made on the variable p_{tot} which, for each event, is the sum of the momentum of the trigger proton and the longitudinal energy in the UA2 calorimeter on the trigger side. Since the initial beam momentum was 315 GeV, events with p_{tot} significantly larger than this value must be due to pileup

To illustrate the effectiveness of the first three offline cuts, the distribution in p_{tot} is shown in Fig. 12. The unshaded histogram in this figure shows the distribution of p_{tot} for a sample of events from the Proton-ΣE_t trigger (see Table 1) for which no pileup cuts have been applied. The shaded histogram shows the subset of those events for which the first three conditions are satisfied. The events with $p_{tot} > 320$ GeV are removed with a final cut. A pileup suppression factor of about 6 is obtained, with about a 10% loss of signal.

Halo Rejection Halo background (non-interacted beam tracks which traverse a spectrometer) is easily identifiable since the focussing of the beam at the intesection region requires that most outgoing halo particles which are within a spectrometer's acceptance should also have traversed the diagonally opposite spectrometer before arriving at the interaction region. This background was partially suppressed at the trigger level by the scintillator vetoes described in Section 3.5, but a significant number of events containing halo tracks were found to remain, primarily in the Proton trigger.

Halo events are suppressed offline by demanding that no chamber in the spectrometer diagonally opposite the trigger spectrometer contain an early (zero drift time) hit. We also require that all good tracks be consistent with originating at the intersection region, in order to suppress the small number of halo tracks which do not pass through the opposite spectrometer. These two cuts remove 14% of all Proton triggers, but less than 1% of Proton-ΣE_t triggers, which have less contamination because of the transverse energy requirement.

6 System Performance

6.1 Trigger Efficiencies

The efficiencies for each of the trigger requirements listed in Sect. 3.5 (with the exception

of the ΣE_t condition) were determined primarily by studying data samples taken with the requirement in question removed from the trigger. As an example, the efficiencies for each of the Proton trigger requirements are shown in Table 2. Additional inefficiencies such as those caused by the ΣE_t requirement and offline cuts are discussed in forthcoming publications [4, 5, 6].

EDSEL Efficiency Causes of EDSEL losses include chamber inefficiencies, extra hits from second tracks (due to either pileup or beam halo), and clusters of three or more adjacent hits caused by δ-ray emission. EDSEL also vetoes events which have chamber hits caused by low-momentum tracks produced in the same interaction and in the same spectrometer. However, these are excluded from the EDSEL efficiency calculation, because the physics interest in Proton trigger events requires a rapididity gap between the observed trigger proton and other tracks. EDSEL inefficiency from pileup is small and is treated as a statistical correction.

Away from the chamber edges, where hit efficiencies are large, EDSEL inefficiencies due to missed hits is approximately 2%. In the cross-section analyses, this source of inefficiency is corrected for by EDSEL emulation in the UA8 Monte Carlo program.

The remaining EDSEL inefficiency due to halo and δ-ray emission is estimated to be $\sim$9%, using a data sample collected without imposing the EDSEL and DIMSUM trigger requirements.

DIMSUM Efficiency The DIMSUM efficiencies were calculated for each spectrometer by using a data sample collected without imposing the DIMSUM trigger requirement. The DIMSUM trigger decision was emulated in an offline analysis of these data and the efficiency was tabulated versus track momentum for each DIMSUM range. This efficiency was found to always be larger than 97% for all spectrometers.

Halo Veto and Opposite Veto Corrections The losses due to accidental vetoes by halo or opposite veto logic are much less than 1% for all spectrometers and are therefore negligible.

6.2 Resolutions

Fig. 13 shows the momentum distribution for a sample of Elastic-trigger events. The curve is a Gaussian fit with σ = 1.9 GeV, in good agreement with Monte Carlo expectations. When fitting the elastic tracks, a primary vertex point at the center of the intersection region is assumed. This results in a resolution 50% better than if only the chamber hits are used.

The online momentum resolution of the trigger processor is illustrated in Fig. 14 which shows the difference between the offline and online momentum calculations for a sample of Proton trigger events. The Gaussian fit with σ = 4.4 GeV implies a processor momentum resolution of 4.0 GeV or 1.4%. The fact that this resolution is worse than the offline resolution of 0.6% stems from the facts that the primary vertex point was not used in the online algorithm and that the offline estimate benefits from further improved chamber alignment and drift time

corrections. However, there is no reason why a primary vertex point could not be used in any future experiment of this type. The distribution in Fig. 14 does not peak at zero because of small errors in the chamber positions which were used to compute the DIMSUM tables used online.

Our t resolution is limited by the beam divergence of about 0.16 mrad. For events with a detected vertex, the contribution from measurement error of the scattered particle is negligible. For events without a detected vertex, the angular resolution gives a contribution of about 20% of the beam dispersion. Using the relation $t \sim p_t^2$ (valid at $x_p = 1$), we estimate that the t resolution due to beam divergence varies from 0.10 to 0.16 GeV^2 over the accepted range. The systematic t-scale uncertainty due to limited knowledge of the Roman pot alignment constants is estimated to be 0.024 (0.038) GeV^2 for t of 1.0 (2.5) GeV^2.

7 Conclusions

We have described the apparatus used by experiment UA8 at the CERN Sp$\bar{p}$S-Collider to isolate and trigger on events which contained leading protons or antiprotons observed at small angles. Data were taken in conjunction with UA2 during collider runs in 1985 and 1987-1989. The interface between the UA8 and UA2 experiments allowed UA8 to use information from the UA2 calorimeters in the trigger decision, and also made it possible for the spectrometer data to be written onto UA2 data tapes together with data from the UA2 apparatus.

The performance of the UA8 spectrometers was satisfactory. The mini-drift chambers achieved a point resolution of 65 μm in the bending view. The momentum resolution was 0.6% at 315 GeV. Several of the UA8 triggers relied on a data-driven processor embedded in the high bandwidth TDC readout system, which provided relatively precise reconstructed and calculated momentum vectors of tracks in the Roman pot spectrometers less than 1.3 μsec after arrival of the bunch crossing signal in the counting room. The efficient triggering scheme allowed UA8 to obtain a large data sample without unacceptably perturbing the UA2 physics program.

8 Acknowledgements

We thank P. Darriulat and A. Donnachie for their support of Experiment UA8. We are indebted to the entire UA2 collaboration for the friendly cooperation which made this experiment possible and, in particular, to John R. Hansen, Sten Hellman, Livio Mapelli and Kevin Einsweiler, who gave generously of their time to help us interface UA8 to UA2. We thank R. Bonino for his contributions to the early phase of UA8 and R. Maleyran for his valuable help in designing the interface between our detectors and the Roman pots. We are also grateful to Al Casillas and the Mechanical Shop of the UCLA Physics Department, where the wire chambers and their supports were fabricated, and to Zak Sandler and the Electronics Shop for assistence

in the design and production of the LOGICBOX module. We thank G. Muratori for extending to us the hospitality of his shop at CERN for wiring and assembling our chambers. Finally, we express our gratitude to Bill Sippach for suggesting the data-driven trigger processing approach.

References

[1] C. N. Booth (UA2 Collaboration), Proceedings of the 6th Topical Workshop on Proton-Antiproton Collider Physics (Aachen 1986), eds. K. Eggert et al. (World Scientific, Singapore, 1987) p. 381; A. Beer et al., Nucl. Instruments & Methods 224 (1984) 360.

[2] J. G. Zweizig et al. (UA8 Collaboration), Nucl. Instruments & Methods A263 (1988) 188.

[3] R. Bonino et al. (UA8 Collaboration), Phys. Letters 211B (1988) 239.

[4] A. Brandt et al. (UA8 Collaboration), "Evidence For A Super-Hard Pomeron Structure", Phys. Letters (in press - 1992).

[5] A. Brandt et al. (UA8 Collaboration), "Properties of Single Diffractive Excitation in $p\bar{p}$ Interactions with $\sqrt{s} = 630$ GeV", to be submitted to Phys. Review D.

[6] A. Brandt et al. (UA8 Collaboration), "Properties of Double Pomeron Exchange in $p\bar{p}$ Interactions with $\sqrt{s} = 630$ GeV", to be submitted to Phys. Review D.

[7] A. Brandt et al. (UA8 Collaboration), "Measurements of Inclusive $\overline{\Lambda^0}$ Production with Large x_F at the Sp$\bar{p}$S-Collider", to be submitted to Zeitschrift f. Phys C.

[8] J. Buskens et al. (UA4 Collaboration), Nucl. Instruments & Methods 207 (1983) 365.

[9] P. J. Ponting, A Guide to the Romulus/Remus Data Acquisition System, CERN-EP-EL Note 80-01 (CAMAC Note 310), (1980).

[10] A. Oreve and J. P. Vanuxem, CERN CAMAC (EP-EL) Note 71-00 (1980).

[11] P. Chauvat et. al., "The Performance of a 16,000 Wire Mini-Drift MWPC System", Proceedings of the 1983 DPF Workshop on Collider Detectors, LBL-15973, page 81; see also, for example, Phys. Letters 127B (1983) 384 and 199 (1987) 304.

[12] J. Ellett, R. Jackson and J. G. Zweizig, "The TDC Buffer Readout Controller", UCLA-VIRTUS/86-01; "The Dual Input Memory-Lookup and Summation Module, DIMSUM", UCLA-VIRTUS/86-02; "The Event Data Selection Module, EDSEL", UCLA-VIRTUS/86-03.

[13] K. L. Brown et al., "TRANSPORT, A Computer Program for Designing Charged Particle Beam Transport Systems", CERN 80-04.

Trigger Name	No. Tracks	ΣE_t (GeV)	Other Conditions (t in GeV^2)	Raw Rates per 10^{30}
Beam-Crossing				260,000
Minimum Bias-ΣE_t		> 18		4,626
Proton	1		$1.05 > x_p > 0.70$	22.7
Proton-ΣE_t	1	> 18	$1.05 > x_p > 0.70$	1.01
Proton-$\Sigma E_t'$	1	> 30	$0.95 > x_p$	0.096
High-t	1	> 18	$\|t\| > 1.7$, $1.05 > x_p > 0.90$	0.034
Double-Pomeron	2		Tracks either in both upper or both lower spectrometers.	0.002
Elastic Scattering	2		Tracks in diagonally opposite spectrometers.	0.040

Table 1: UA8 trigger names and requirements. A Beam-Crossing (RF) signal was required in all triggers. The Raw Rates are given in units of Hz per Luminosity of $10^{30}\,\mathrm{cm}^{-2}\,\mathrm{sec}^{-1}$.

	PU	PD	MU	MD
EDSEL	.902	.924	.907	.895
DIMSUM	.974	.970	.976	.993
Halo Veto	.995	.995	.998	.998
Opposite Veto	.998	.998	.997	.997

Table 2: Efficiencies by spectrometer for Proton trigger

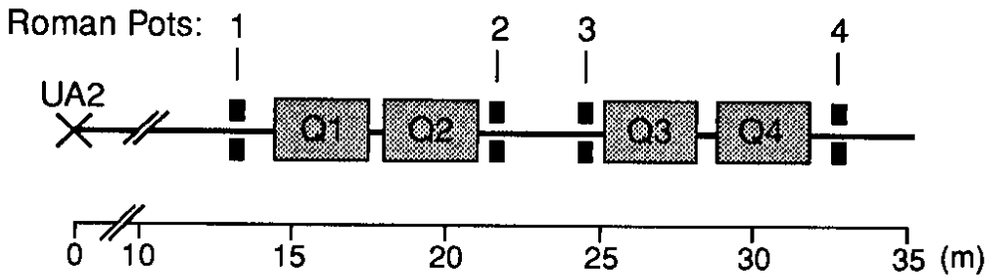

Figure 1: The UA8 apparatus. There are four Roman pots above and four below the beam line in each arm. (Only one arm is shown here.) The machine quadrupoles (labeled Q1, Q2, Q3 and Q4) are used for momentum analysis. Distances shown are measured from the bunch-crossing center. The UA2 detector is at the center of the interaction region.

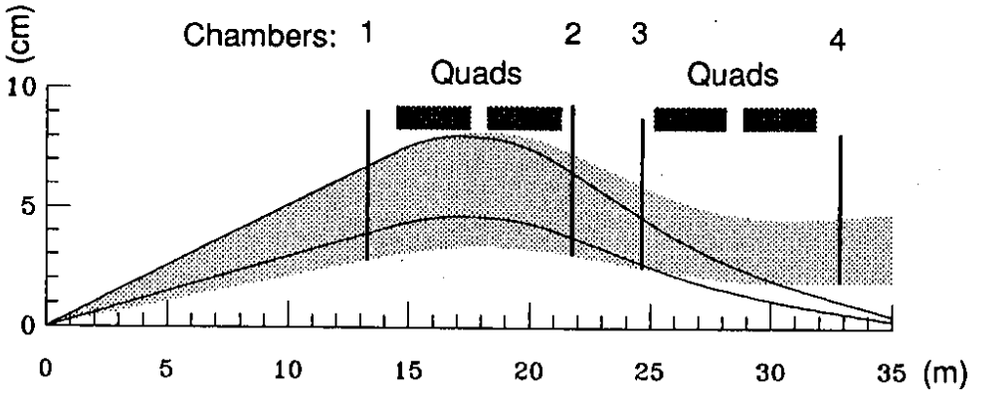

Figure 2: Particle trajectories through a Roman pot spectrometer. The solid curves show the trajectories of 300 GeV particles emerging from the center of the intersection region with minimum and maximum acceptable angles. The lower edge of the shaded region is 12 beam widths (σ) from the beam orbit center and coincides with the trajectory of the smallest angle elastic track accepted, while the upper edge corresponds to the trajectory of the largest angle elastic track which remains inside the vacuum pipe.

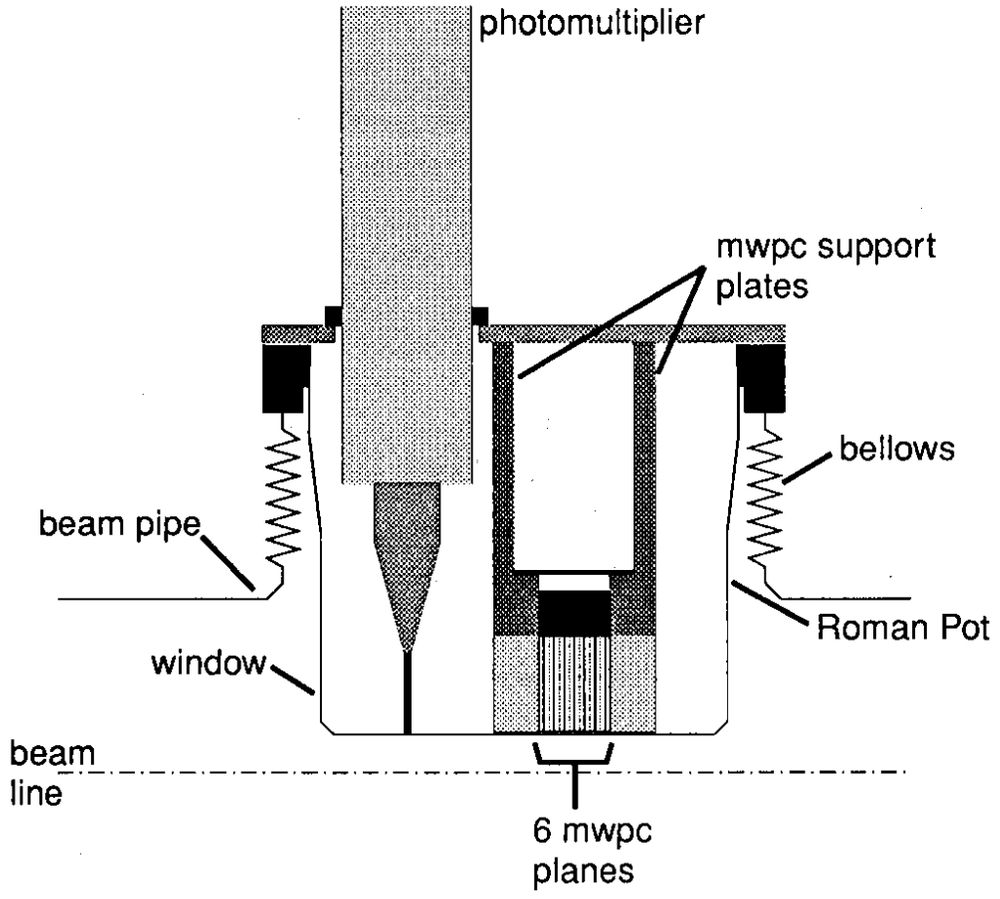

Figure 3: A vertical slice through a Roman pot and detector assembly. The mini-drift chamber hangs from a circular top flange, the bottom edge of which provides the reference level and is mounted flush with a corresponding reference plate on the Roman pot support. Particles emerging from interactions traverse from the right and pass though 100μm thick stainless steel windows upon entrance and exit of the pot. The bellows allow the pot to be retracted by 8cm during periods of beam instability.

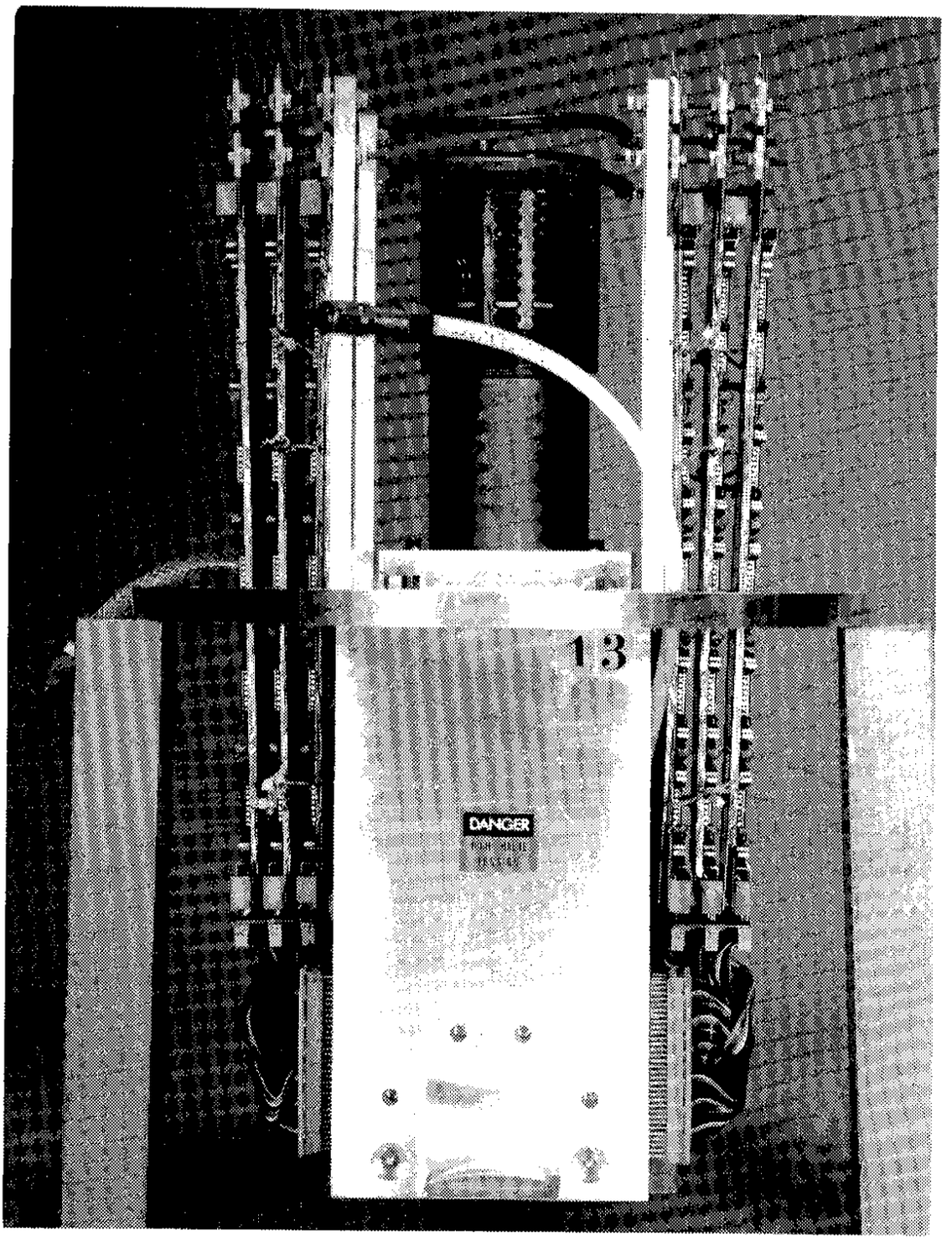

Figure 4: Photograph of a Roman pot detector assembly. On either side of the chamber are three circuit boards which hold the amplifiers and comparators for anode signals. Short lengths of flat ribbon cable connect the pre-amplifier inputs to the card-edge connectors. The photomultiplier shielding is visible above the mounting flange.

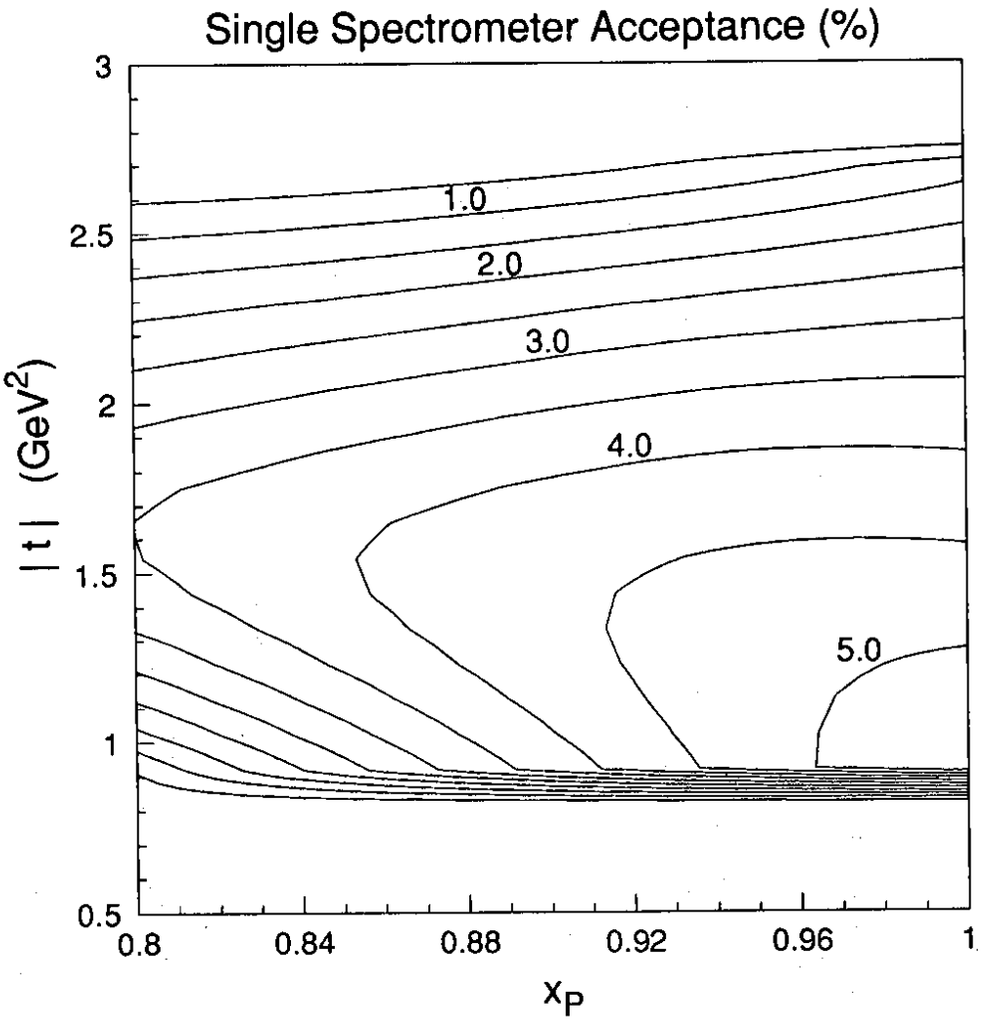

Figure 5: Acceptance contours for one Roman pot spectrometer, calculated assuming $12\,\sigma$ pot positions. Contours are labled with percentage acceptance. Acceptance extended from 0.8 to 2.5 GeV^2 in t and down to 0.7 in x_p.

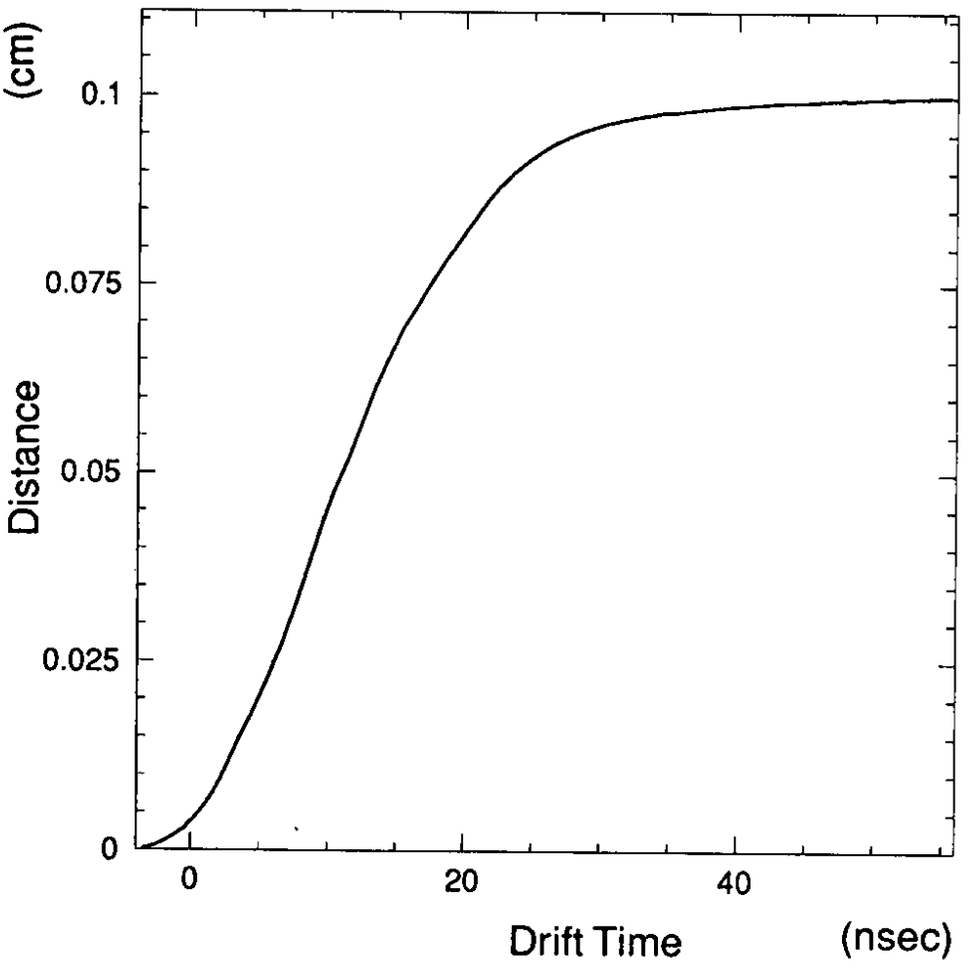

Figure 6: The most likely distance between the point-of impact of a track on an anode plane from the hit anode wire vs. corrected drift time for a 2 mm MWPC cell. The curve is calculated as described in the text.

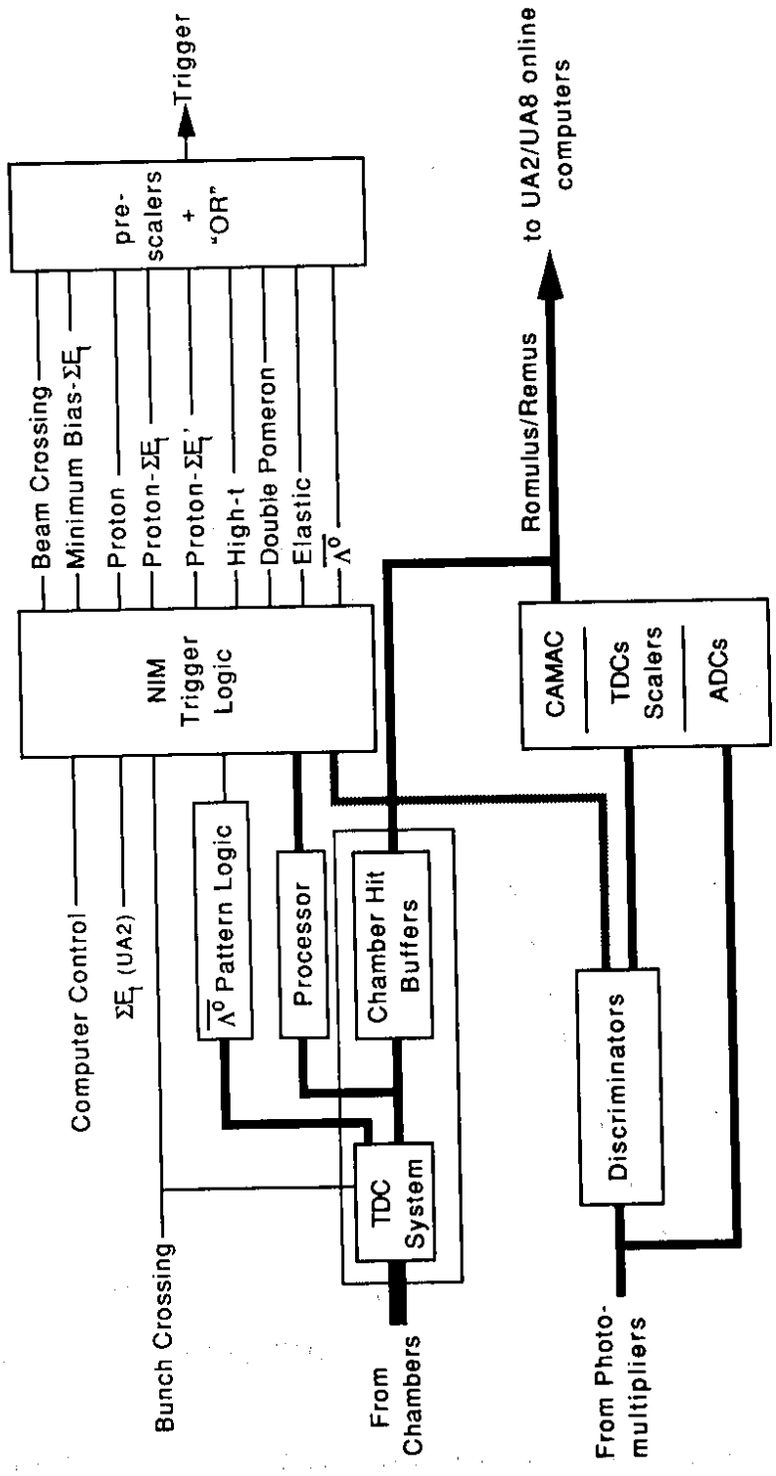

Figure 7: Block diagram of the UA8 trigger system. Chamber hits are latched in the TDC system, then tranferred to hit buffers and a data-driven processor which finds tracks, computes momenta, momentum transfers and intercepts. This information is combined with scintillator hit information, the ΣE_t signal from the UA2 calorimeter and a beam crossing signal to produce 8 independent trigger decisions, which were OR'ed together to form a global trigger. A ninth trigger used pattern matching logic to trigger on $\overline{\Lambda^\circ}$'s in the spectrometers.

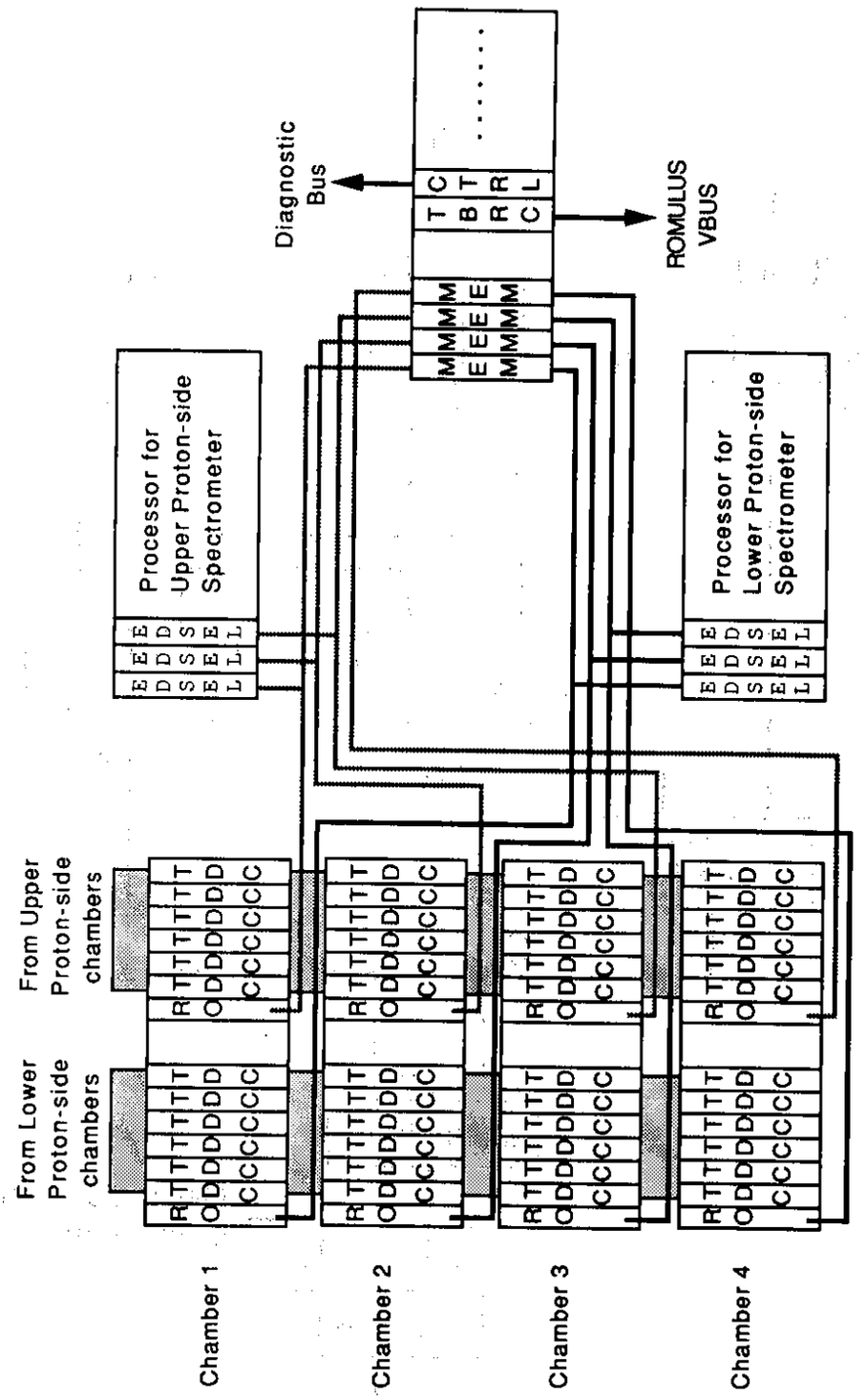

Figure 8: Block diagram of the TDC, Processor and Hit-Buffer System (proton side only). Flat polyethylene cables transmit amplified chamber signals to the TDC modules, where their Gray-coded arrival times are latched. Readout for all chambers proceeds in parallel from the Readout ("RO") modules to the Memory ("MEM") modules under the control of the "CTRL" module. Hits from y and $\tilde{y}$ planes are simultaneously latched in the "EDSEL" modules for the data-driven processor. The Diagnostic Bus is interfaced to the μVAX online computer through a parallel interface in CAMAC.

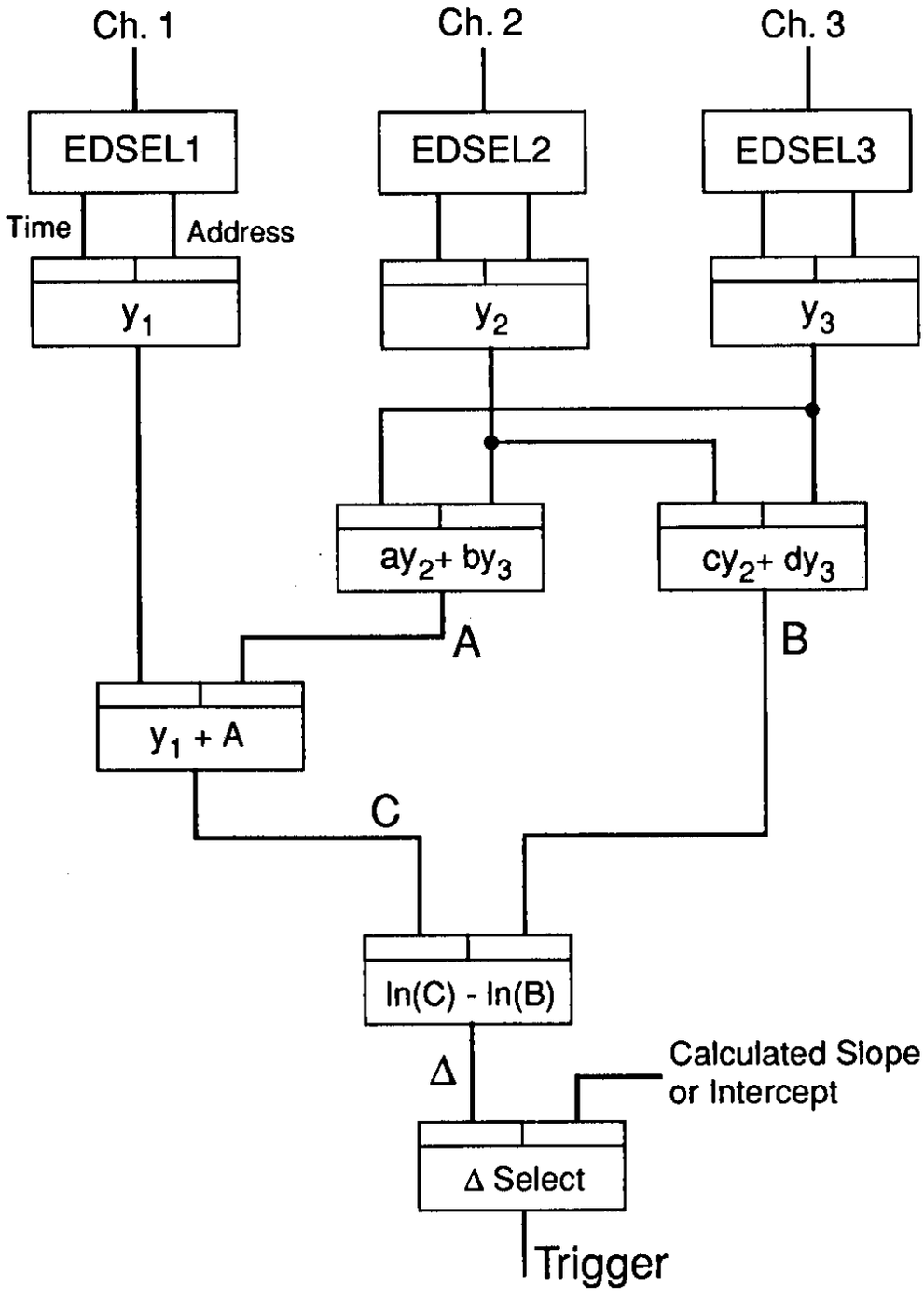

Figure 9: UA8 data-driven trigger processor block diagram. Chamber hits are latched in the top row of modules (EDSEL). All other modules are DIMSUM modules. The top row of DIMSUM modules computes hit coordinates which are input into modules which execute the algorithm explained in the text. The slope and intercept calculations are not shown. The bottom module selects tracks with momenta and slope/intercept in one of three different sets of ranges of these variables, as explained in the text.

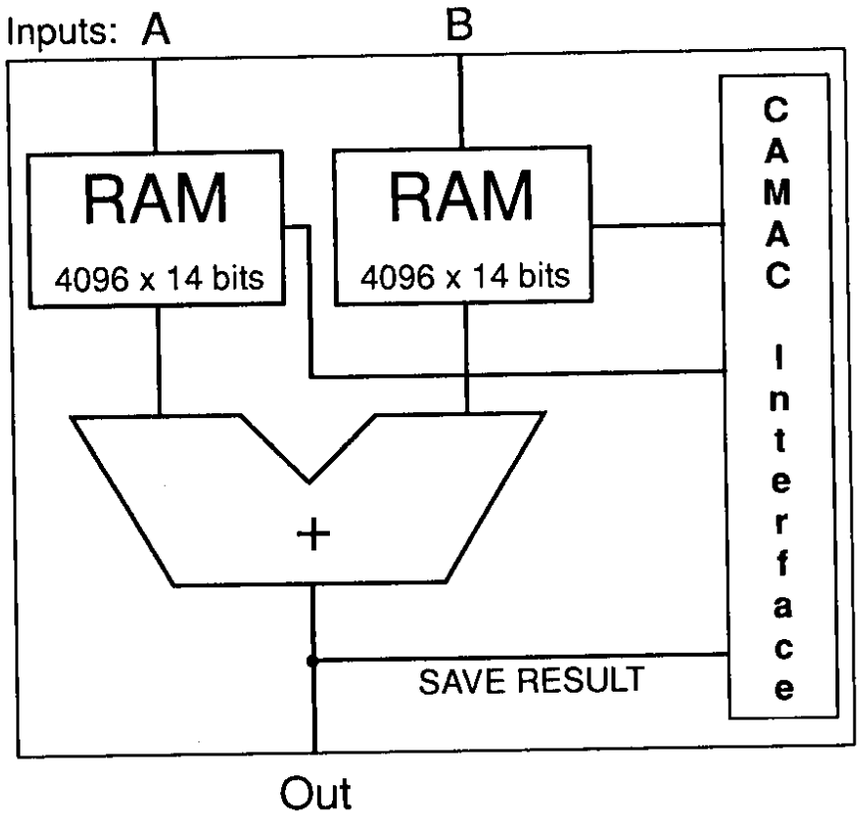

Figure 10: Block diagram of the DIMSUM Module. Each 12-bit input addresses a 4096 x 14 bit RAM. The first 12 bits of each addressed word are summed and the result is output on a 12-bit bus. The two additional bits contain a parity bit and an Invalid-Operand flag. RAM data can be entered or read via the CAMAC interface. Fast inputs and output are via front panel connections.

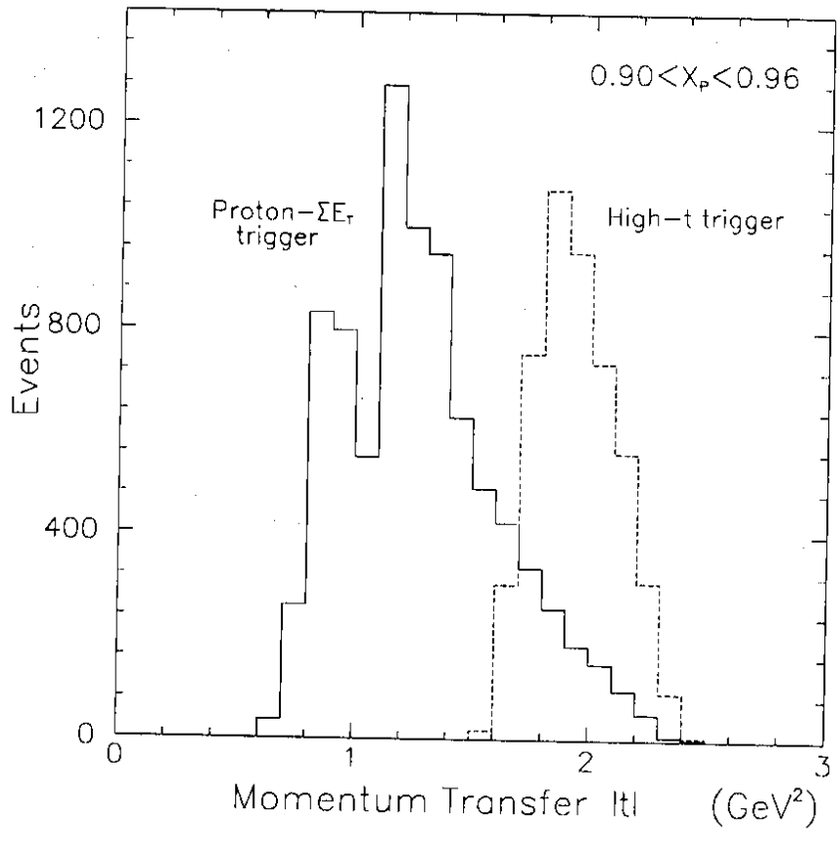

Figure 11: The total raw 4-momentum transfer, t, for all spectrometers calculated offline. The double peaked structure at smaller t arises because the four spectrometers did not have the same minimum accepted t. The dotted histogram, with arbitrary normalization, contains those events which satisfied the High-t trigger requirement.

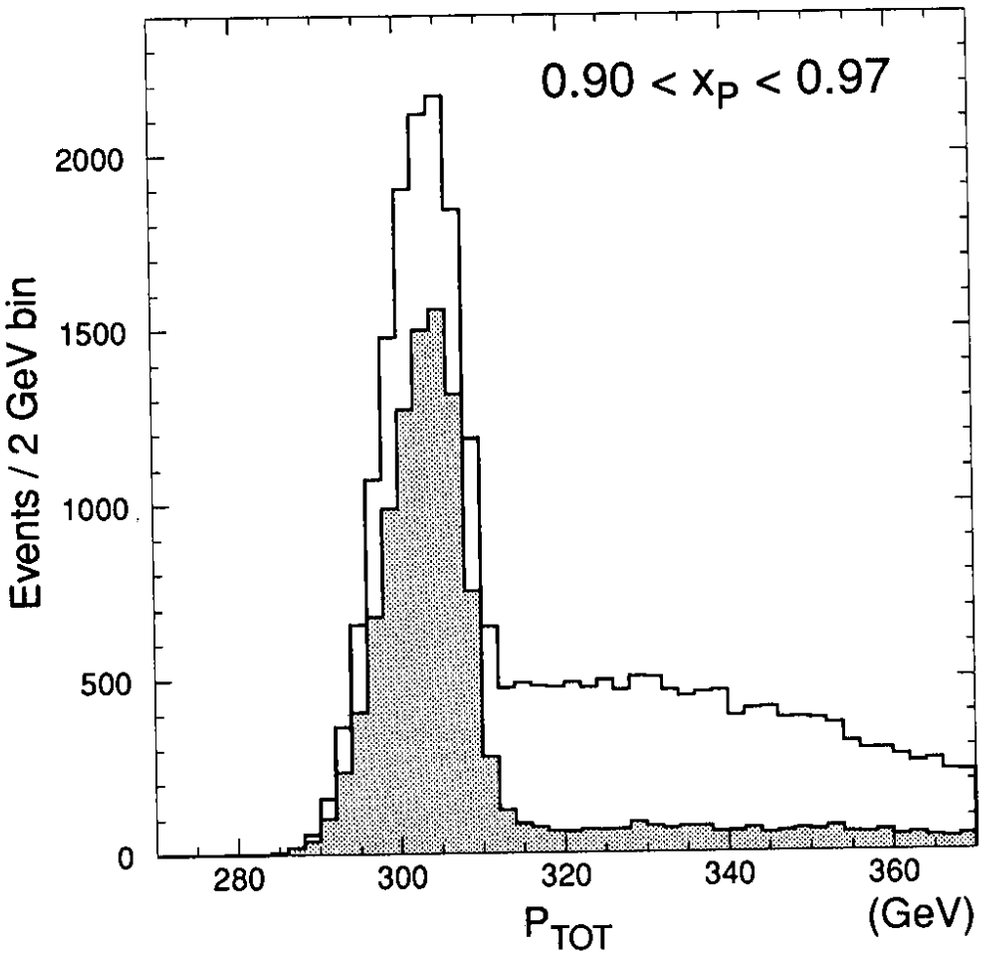

Figure 12: p_{tot} is the offline sum of the momentum of the trigger proton and the longitudinal energy in the UA2 calorimeter on the trigger side. The tail on the right hand side is due to pileup. The shaded events remain after the application of TOF and silicon cuts described in the text. The average luminosity was $10^{30}\,\mathrm{cm}^{-2}\,\mathrm{sec}^{-1}$ while these data were being recorded.

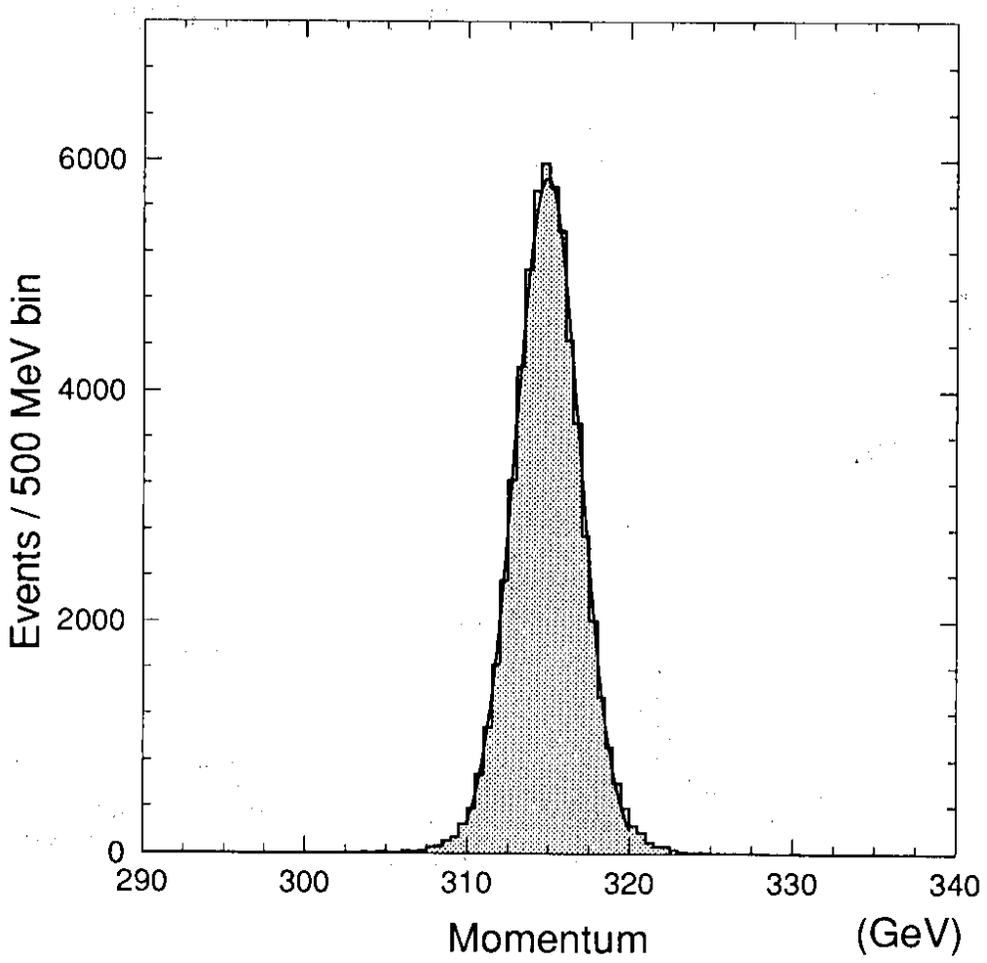

Figure 13: The momentum distribution for a sample of Elastic-trigger tracks. The curve is a Gaussian fit with $\sigma = 1.9$ GeV.

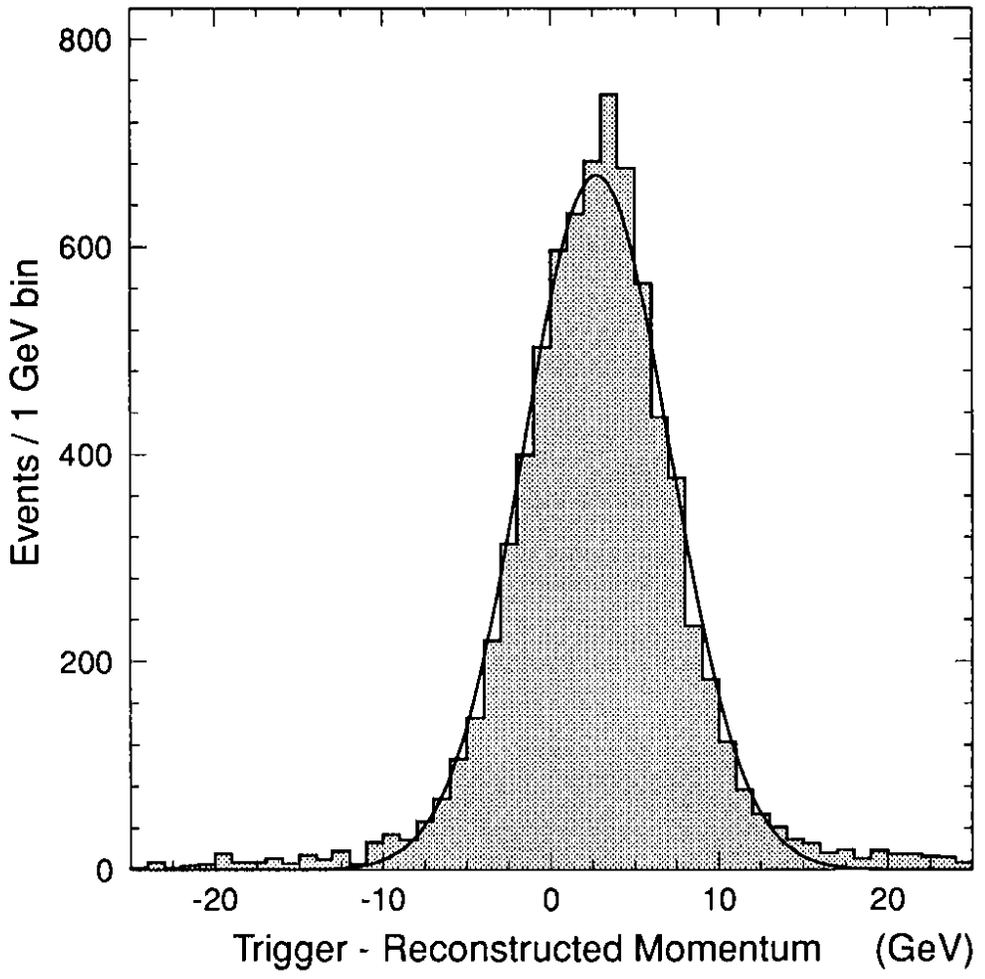

Figure 14: Distribution of the differences between momentum calculations made by the trigger processor and in offline analysis. The curve is a Gaussian fit with $\sigma = 4.4$ GeV. The offset mean value is discussed in the text.